RSC Advances

PAPER

View Article Online
View Journal | View Issue

Cite this: *RSC Adv.*, 2022, **12**, 4946

Improved microstructure and significantly enhanced dielectric properties of $Al^{3+}/Cr^{3+}/Ta^{5+}$ triple-doped TiO_2 ceramics by Re-balancing charge compensation

Porntip Siriya,[a] Atip Pengpad,[a] Pornjuk Srepusharawoot,[a] Narong Chanlek[b] and Prasit Thongbai *[a]

The charge compensation mechanism and dielectric properties of the $(Al_xCr_{0.05-x})Ta_{0.05}Ti_{0.9}O_2$ ceramics were studied. The mean grain size slightly changed with the increase in the Al^{3+}/Cr^{3+} ratio, while the porosity was significantly reduced. The dielectric permittivity of the co-doped $Cr_{0.05}Ta_{0.05}Ti_{0.9}O_2$ ceramic was as low as $\varepsilon' \sim 10^3$, which was described by self-charge compensation between Cr^{3+}–Ta^{5+}, suppressing the formation of Ti^{3+}. Interestingly, ε' can be significantly increased (6.68×10^4) by re-balancing the charge compensation *via* triple doping with Al^{3+} in the Al^{3+}/Cr^{3+} ratio of 1.0, while a low loss tangent (~0.07) was obtained. The insulating grains of $[Cr_{0.05}{}^{3+}Ta_{0.05}{}^{5+}]Ti_{0.9}{}^{4+}O_{12}$ has become the semiconducting grains for the triple-doped $Al_x{}^{3+}[Cr_{0.05-x}{}^{3+}Ta_{0.05-x}{}^{5+}][Ta_x{}^{5+}Ti_x{}^{3+}Ti_{0.9+x}{}^{4+}]O_{12+3x/2}$. Considering an insulating grain with low ε' of the $Cr_{0.05}Ta_{0.05}Ti_{0.9}O_2$ ceramic, the electron-pinned defect-dipoles and interfacial polarization were unlikely to exist supported by the first principles calculations. The significantly enhanced ε' value of the triple-doped ceramic was primarily contributed by the interfacial polarization at the interface between the semiconducting and insulating parts, which was supported by impedance spectroscopy. This research gives an underlying mechanism on the charge compensation in the $Al^{3+}/Cr^{3+}/Ta^{5+}$-doped TiO_2 system for further designing the dielectric and electrical properties of TiO_2-based ceramics for capacitor applications.

Received 5th December 2021
Accepted 25th January 2022

DOI: 10.1039/d1ra08847e

rsc.li/rsc-advances

1. Introduction

Recently, a large number of accepter/donor co-doped TiO_2 ceramics have been widely investigated due to a potential application in ceramic capacitors such as In^{3+}/Nb^{5+},[1–4] Al^{3+}/Nb^{5+},[5–7] Ga^{3+}/Nb^{5+},[8,9] Sc^{3+}/Nb^{5+},[10] Fe^{3+}/Nb^{5+},[11,12] Er^{3+}/Nb^{5+},[13,14] Zn^{2+}/Nb^{5+},[15,16] Dy^{3+}/Nb^{5+},[17] Gd^{3+}/Nb^{5+},[18] Mg^{2+}/Nb^{5+},[19,20] Ag^{+}/Nb^{5+},[21,22] Li^{+}/Nb^{5+},[23] Pr^{3+}/Nb^{5+},[24] Ga^{3+}/Ta^{5+},[25] Al^{3+}/Ta^{5+},[26] Mg^{2+}/Ta^{5+},[27,28] Co^{2+}/Nb^{5+},[29] and Bi^{3+}/Sb^{5+} (ref. 30) co-doped TiO_2 ceramics. All these ceramic systems exhibited a high dielectric constant ($\varepsilon' > 10^4$), low loss tangent ($\tan\delta < 0.1$), and good temperature stability of ε'. The giant dielectric (GD) behavior of these co-doped TiO_2 systems have been explained using several models such as electron-pinned defect-dipoles (EPDDs),[1,16,28] surface barrier layer capacitors (SBLCs),[31,32] internal barrier layer capacitors (IBLCs),[33–36] and small polaron hopping models.[8]

According to the previous studies, the Al^{3+}/Nb^{5+} (ANTO) and Al^{3+}/Ta^{5+} co-doped TiO_2 (ATTO) ceramics with different co-doping concentrations can exhibit a high ε' (>10^4) and low $\tan\delta$ (<0.05).[5–7,26] Using impedance spectroscopy, the semi-circular arc of the grain (R_g) and grain boundary (R_{gb}) were found, which $R_g \ll R_{gb}$.[5,7,26] This means that the GD response of the ATTO ceramics is caused by the interfacial polarization between the semiconducting and insulating parts. On the other hand, the observed GD response with low $\tan\delta$ in the Al^{3+}/Nb^{5+} co-doped TiO_2 (ANTO) with various co-doping concentrations.[6] It was clearly demonstrated that the surface layer on the ANTO has a remarkable impact on the $\tan\delta$ value, which would be increased after removing the surface layer. Accordingly, the important role of Al^{3+} is to form the insulative surface layer without the formation of oxygen vacancies.[6] The GD response in the ANTO was further shown to be caused by the insulating grain boundaries (GBs),[5,7] whereas the low $\tan\delta$ was due to the synergistic effect of insulating GBs (IBLC) and insulative surface layer (SBLC).[5–7,26]

Most recently, the high ε' (>10^4), low $\tan\delta$ (~0.06) as well as the ε' value can be stable in the temperature range from −60 to 150 °C were achieved in the 1.0%Cr^{3+}/Ta^{5+} co-doped TiO_2 ceramics (1% CTTO).[37] According to the first principles

[a]*Giant Dielectric and Computational Design Research Group (GD-CDR), Department of Physics, Faculty of Science, Khon Kaen University, Khon Kaen 40002, Thailand. E-mail: pthongbai@kku.ac.th*

[b]*Synchrotron Light Research Institute (Public Organization), 111 University Avenue, Muang District, Nakhon Ratchasima 30000, Thailand*

calculation and impedance spectroscopy, the GD properties of 1% CTTO were not attributed to the EPDD effect but can be described by internal polarization at the internal interfaces following the IBLC and SBLC effects. It was also found that the GD response in the CTTO decreased with the increase in the co-doping concentration, which might be due to the self-change compensation between the Cr^{3+} and Ta^{5+} doping ions as the co-doping concentration increased.[37] Unfortunately, this issue has never been discussed in detail. On the other hand, the GD responses of the ATTO and ANTO tended to increase with the increase in the co-doping concentration,[5,26] which might be due to the interstitial Al^{3+} ions. The formation of defects and charge compensation in rutile-TiO_2 ceramics has great effects on their dielectric and electrical properties. Thus, it is important to study the possible mechanisms of the charge compensations in different co-doped TiO_2 systems, which have different defect formations, to better understand the defect formation in co-doped rutile-TiO_2 ceramics.

In the present study, the dielectric and electrical properties of $Al^{3+}/Cr^{3+}/Ta^{5+}$ triple-doped TiO_2 ceramics with various Al^{3+}/Cr^{3+} doping ratios have been investigated. Their phase composition, microstructure, and chemical composition were systematically analyzed. Notably, a low ε' value at 1 kHz of the Cr^{3+}/Ta^{5+} co-doped TiO_2 ceramic ($\sim 1 \times 10^3$) owing to the self-charge compensation between the dopants was greatly enhanced to 6.68×10^4 by triple doping with Al^{3+}, which was due to the re-balance of the charge compensation. Furthermore, the tan δ value at 1 kHz was decreased from 0.239 to 0.070.

2. Experimental details

Triple-doped $Al_xCr_{0.05-x}Ta_{0.05}Ti_{0.9}O_2$ ceramics with $x = 0$, 0.005, and 0.025, (abbreviated as the CTTO, ACTTO-1 and ACTTO-2, respectively) were prepared by a conventional solid–state reaction method. TiO_2 (Sigma-Aldrich, >99.9% purity), Al_2O_3 (Sigma-Aldrich, 99.99% purity), Cr_2O_3 (Sigma-Aldrich, ≥98% purity), and Ta_2O_5 (Sigma-Aldrich, 99.99% purity) were used as the starting raw materials. A wet ball milling method was used to mix the starting oxides. First, the starting raw oxides (~10 g) were mixed by the ball milling method in ethanol (50 mL) for 24 h using ZrO_2 balls (2 mm in diameter) as a grinding media. Second, the ZrO_2 balls were separated. Third, ethanol was evaporated in an oven at 90 °C for 24 h. Details of the preparation route were previously reported.[26,37] Next, the mixture of dried powders was pressed into the pellets without calcination. Finally, all the pellet samples were sintered at 1450 °C for 5 h at a heating rate of 3 °C min^{-1} to form the ceramic samples.

The phase composition and crystal structures of the sintered samples were analyzed by X-ray diffraction (XRD, PANalytical, EMPYREAN). Field emission scanning electron microscopy (FESEM, Helios nanoLab, G3 CX) and energy-dispersive X-ray analysis (EDS-Mapping) were used to characterize the surface morphologies and dopant distribution of the ceramic samples, respectively. The oxidation state was investigated by X-ray photoelectron spectroscopy (XPS, AXIS Ultra DLD, UK) at Synchrotron Light Research Institute (SLRI), Thailand.

The parallel plate electrodes on the as-sintered samples were coated with Ag paint by heating at 600 °C for 30 min. The dielectric properties of all the samples were quantified using an impedance analyzer (KEYSIGHT, E4990A) over the frequency and temperature ranges of 10^2–10^6 Hz and −60 to 210 °C, respectively. The impedance calculation of all the ceramic samples was as follows:

$$Z^* = Z' - jZ'' = \frac{1}{R_g^{-1} + j\omega C_g} + \frac{1}{R_g^{-1} + j\omega C_{gb}}, \quad (1)$$

where C_g and C_{gb} are the capacitances of the grain and GB, respectively. The first principle calculation was performed to calculate the formation energy and preferable sites of the dopants in the rutile structure. Details of the first principles calculation were provided in the previous studies.[37,38]

3. Results and discussion

Fig. 1(a) shows the XRD patterns of all sintered ceramics. A rutile-TiO_2 (JCPDS 21-1276)[1,2,16] with no impurity phase was observed in all samples. Fig. 1(b) and (c) display the Rietveld profile fitting for the CTTO, ACTTO-1, and ACTTO-2 ceramics, respectively. The results are well-fitted with the goodness of fit (GOF) of ~1.483–2.127. The lattice parameters (a and c values) and the structural data, which were obtained from the Rietveld refinement, are summarized in Table 1. For the CTTO, the a and c values are larger than those of the undoped TiO_2 ceramic and $Cr_{0.005}Ta_{0.005}Ti_{0.99}O_2$.[37] This result is due to the relatively large ionic radii of the Cr^{3+} ($r_6 = 61.5$ pm) and Ta^{5+} ($r_6 = 64.0$ pm) dopants compared to that of the Ti^{4+} ($r_6 = 60.5$ pm)[39] host ion and a high co-doping concentration. After the replacement of Cr^{3+} with Al^{3+}, the a and c values slightly decreased with the increase in the Al^{3+}/Cr^{3+} ratio concentration because of the relatively low ionic radius of Al^{3+} ($r_6 = 53.5$ pm).[26,39]

The most preferential rutile structure of the rutile-TiO_2 structure doping with Al and Cr was studied *via* first principles calculations. As illustrated in Fig. 2, four different structures (S1–S4) of the Al- or Cr-doped TiO_2 were designed by adding an oxygen vacancy (V_o). The total energies of different structures (S1–S4) were calculated by $\Delta E = E - E(S1)$, where E and $E(S1)$ are total energies of various structures and structure,[1] respectively. For the S1 structure, the triangular-shaped (2Al)V_oTi or (2Cr)V_oTi defect complex was set. This defect structure is the essential part of the EPDD structure,[1] which will be formed only if (2Al)V_oTi or (2Cr)V_oTi was created and correlated to the diamond-shaped $2NbTi^{3+}A_{Ti}$ (A = $Ti^{4+}/Ti^{3+}/In^{3+}$) defect complex.[40] In the S2–S4 structures, the different structures were designed without forming the triangular-shaped defect complex. According to the total energy calculations, the structures S2 and S3 of the Al- or Cr-doped TiO_2 have the lowest total energy, respectively. For the S2 structure of the Al-doped TiO_2, although two Al atoms prefer to occupy close together, they do not prefer to stay with V_o. Accordingly, this result indirectly indicated that the Al atom is an interstitial atom, which does not require V_o for charge compensation.[6] Furthermore, the Cr atoms do not prefer to occupy close together. If V_o exists in the structure of the Cr-doped TiO_2, the Cr atoms do not prefer to

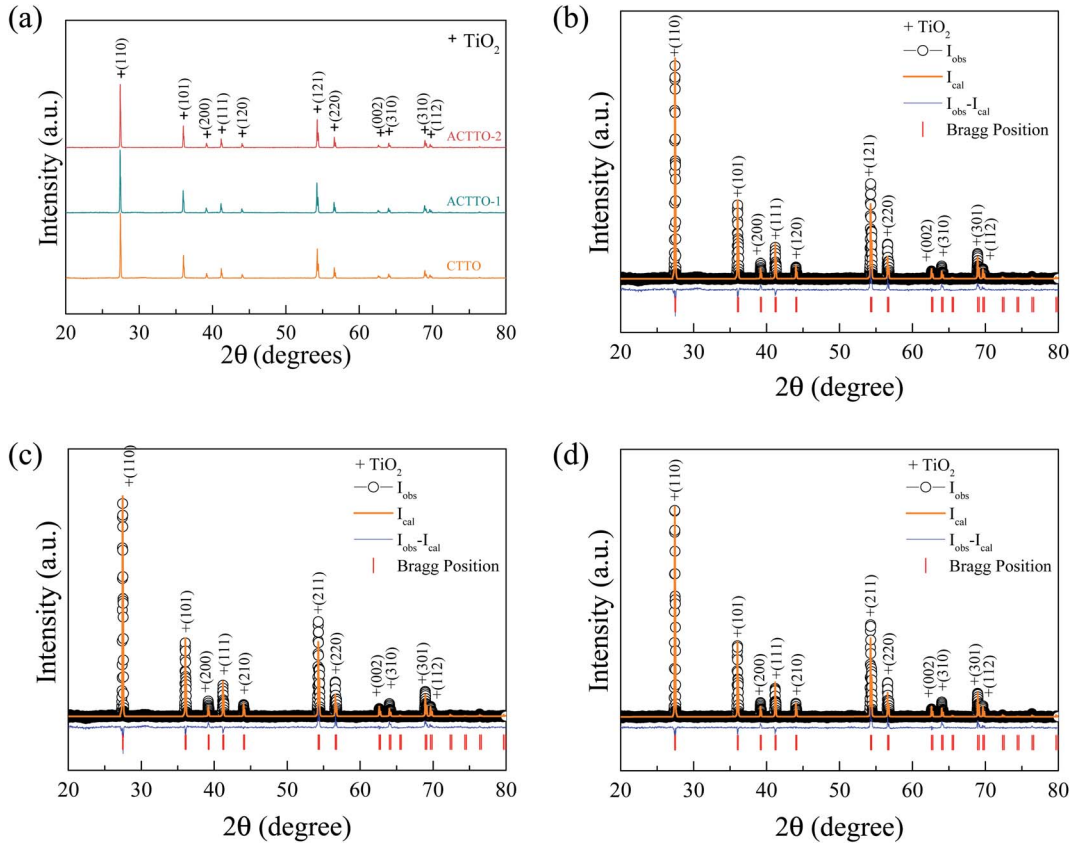

Fig. 1 (a) XRD patterns of CTTO, ACTTO-1, and ACTTO-2 ceramics. (b–d) Rietveld profile fitting for CTTO, ACTTO-1, and ACTTO-2 ceramics, respectively.

stay close to V_o. According to the fundamental concept, EPDDs cannot be formed in the $Al_xCr_{0.05-x}Ta_{0.05}Ti_{0.9}O_2$ structure. Thus, the dielectric properties of $Al_xCr_{0.05-x}Ta_{0.05}Ti_{0.9}O_2$ should be associated with the extrinsic effect of their ceramic microstructure.

As illustrated in Fig. 3, the grain shape of all the ceramics exhibited a relatively similar shape. Numerous small-sized pores in the CTTO ceramic are observed even when the ceramic was sintered at a temperature as high as 1450 °C for 5 h. This observation is in contrast to those reported in other co-doped TiO_2 systems,[9,10,20,21,25,35] which for a highly dense microstructure is usually obtained when sintering at high temperatures >1400 °C. This result indicates that the Cr^{3+} and Ta^{5+} dopants inhibited the sintering (or densification) rate of the TiO_2 ceramic. Usually, the sintering rate of polycrystalline ceramic oxides is dependent on the diffusion rate of ions.[41] The concentration of oxygen vacancies that were produced by the Cr^{3+} doping ions may not be high enough, which might be due to the self-charge compensation between the Cr^{3+} and Ta^{5+} dopants. Then, the number of pores decreased with the increase

Table 1 Structural data obtained by Rietveld refinement, grain size, and relative density for undoped TiO_2, CTTO, ACTTO-1, and ACTTO-2 ceramics

Structural data/Ceramic samples	TiO_2	CTTO	ACTTO-1	ACTTO-2
$a = b$ (Å)	4.591(1)	4.598(0)	4.597(6)	4.594(5)
c (Å)	2.958(9)	2.966(1)	2.966(1)	2.964(5)
GOF	1.483	1.994	2.127	1.815
Bond length (Å), A = Ti, Al, Cr, Ta				
$A_{(0,0,0)}$–$O_{(0.19480,-0.19480,0.50000)}$	1.946(0)	1.950(0)	1.950(0)	1.949(0)
$A_{(0,0,0)}$–$O_{(0.30520,0.30520,0.00000)}$	1.982(0)	1.985(0)	1.984(0)	1.983(0)
$A_{(0,0,0)}$–$O_{(0.30520,-0.69480,0.00000)}$	3.484(0)	3.489(0)	3.489(0)	3.487(0)
$A_{(0,0,0)}$–$A_{(0,0,1)}$	2.959(0)	2.966(0)	2.966(0)	2.964(0)
Grain size (μm)	—	5.8 ± 1.4	5.5 ± 1.5	7.0 ± 2.1
Relative density (%)	—	79.68	80.10	89.03

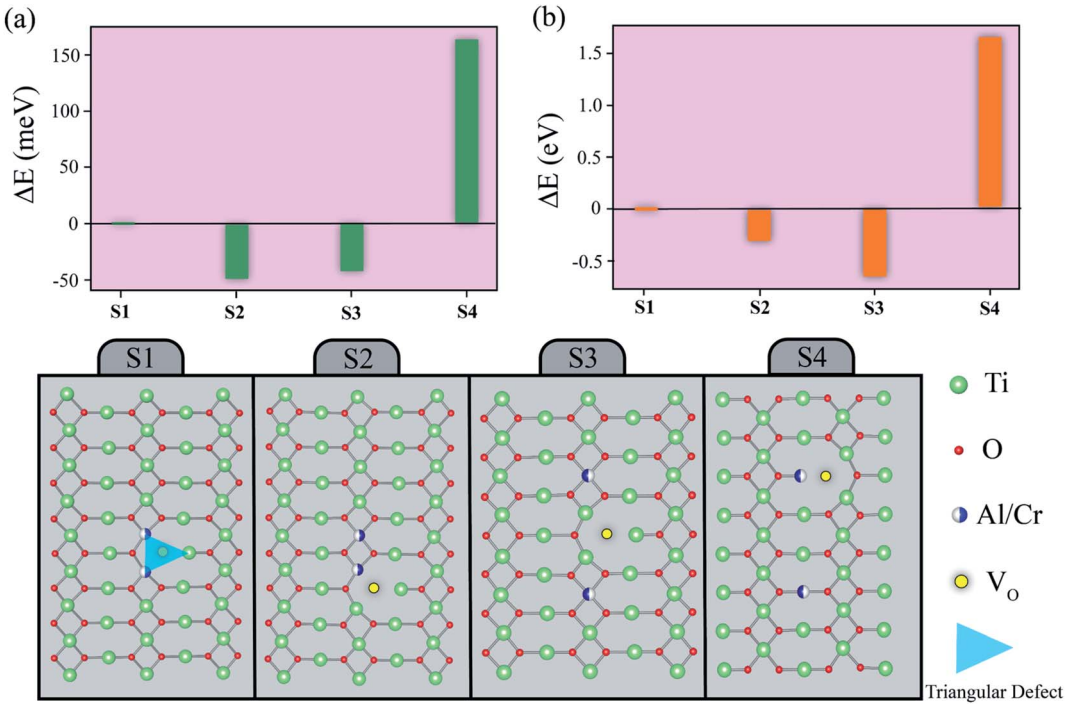

Fig. 2 Total energies of different structures (S1–S4) for TiO_2 substituted with Al and Cr atoms.

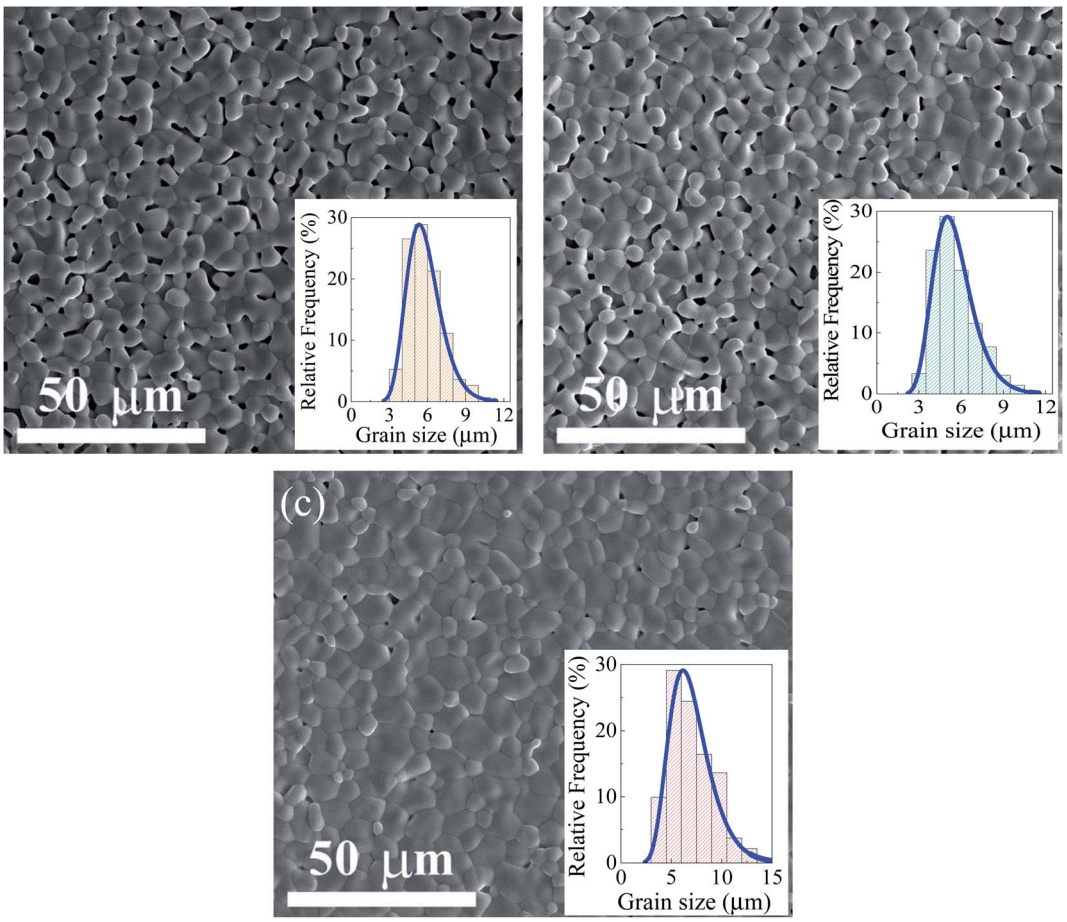

Fig. 3 SEM images of the surface morphologies of (a) CTTO, (b) ACTTO-1, and (c) ACTTO-2 ceramics; insets show their grain size distribution.

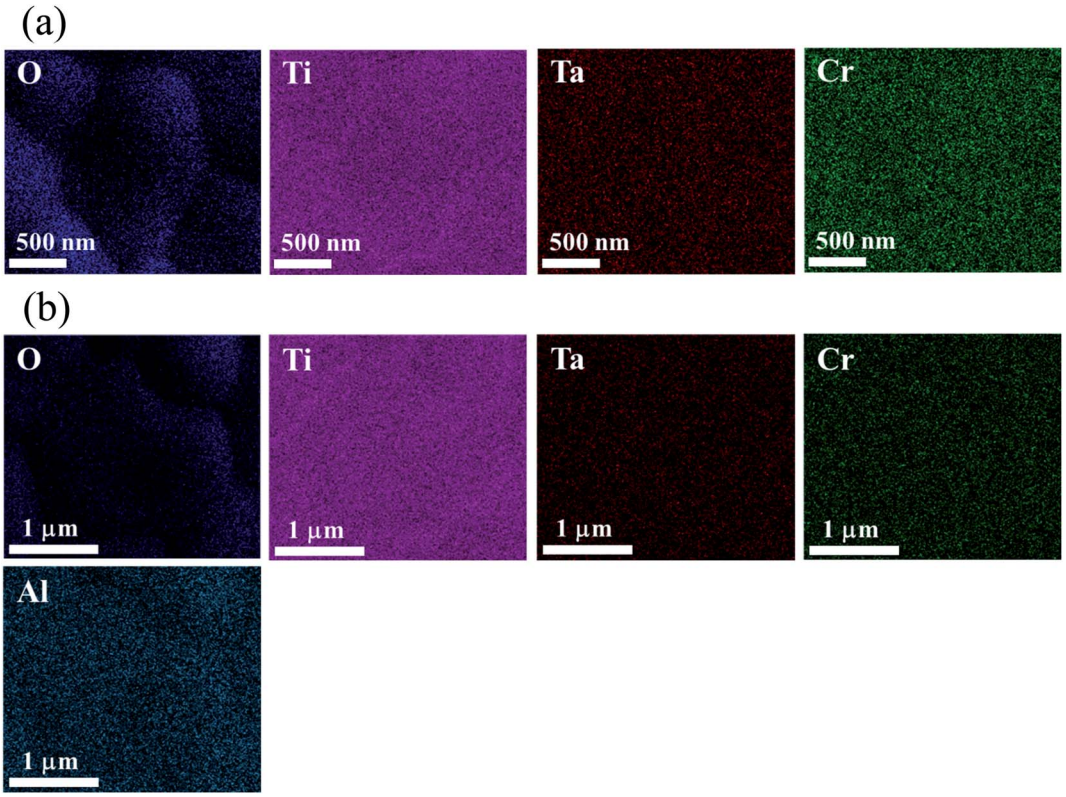

Fig. 4 EDS-SEM mapping images of major and dopant element of (a) CTTO and (b) ACTTO-2 ceramics.

in the Al^{3+}/Cr^{3+} ratio. This result is due to the increase in oxygen vacancies, which will be confirmed by the XPS technique in the next part. As shown in the inset of Fig. 3(a)–(c), the grain size distributions of all the sintered ceramics are narrow. The mean grain sizes of all the sintered ceramics are summarized in Table 1. The mean grain sizes of the CTTO and ACTTO-1 samples are nearly the same, while the mean grain size of the ACTTO-2 sample increased slightly compared to the CTTO sample. This result revealed that the Al^{3+}/Cr^{3+} ratio has a slight effect on the grain growth, but it has a strong effect on the densification process.[41] We reported that the Ta^{5+} dopant has a remarkable effect on the reduction in the grain size of the TiO_2 ceramics,[25,26,37] while the mean grain size of the Al^{3+}-doped TiO_2 was significantly increased compared to that of TiO_2.[26] The slightly increased mean grain size of ACTTO-2 was likely caused by the replacement of Cr^{3+} with Al^{3+}.

As demonstrated in Fig. 4, all dopant elements in the microstructures of the CTTO, which consisted of Cr and Ta dispersed well in both the grain and grain boundary of the CTTO and ACTTO-2. After triple-doping with Al, no segregation of any element in the grains and GBs was observed.

Fig. 5 displays the frequency dependence of ε' (at 25 °C). The dielectric parameters at 1 kHz of all the samples are summarized in Table 2. The ε' values of the CTTO and ACTTO-1 (Al_x-$Cr_{0.05-x}Ta_{0.05}Ti_{0.9}O_2$ with $x = 0.005$, Al^{3+}/Cr^{3+} ratio = 0.11) are nearly the same in value ($\sim 10^3$) over the measured frequency range. The ε' value of the CTTO sintered at 1450 °C, co-doped with 10%(Cr + Ta), was much lower than that of the 1.0%(Cr +

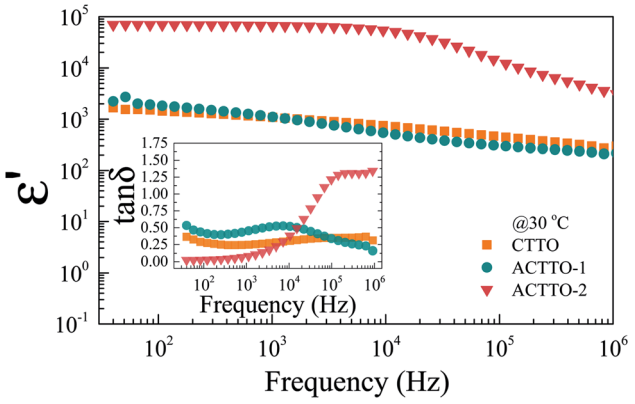

Fig. 5 Frequency dependence of dielectric permittivity (ε') at 30 °C of all ceramics; inset shows the frequency dependence of tan δ at 30 °C.

Table 2 Dielectric permittivity (ε'), loss tangent (tan δ) at 1 kHz, and activation energy of the insulating part (E_i) of all samples

Sample	Dielectric Properties at 30 °C		E_i of the grain (eV)
	ε'	tan δ	
CTTO	1080	0.239	0.705
ACTTO-1	1107	0.442	0.686
ACTTO-2	66 811	0.070	—

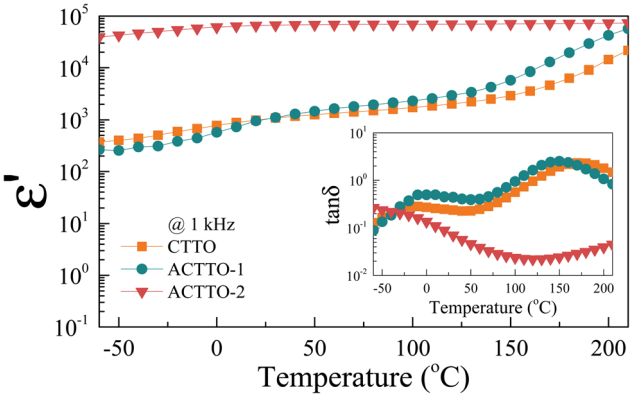

Fig. 6 Temperature dependence of dielectric permittivity (ε') at 10^3 Hz of all ceramics; inset shows the tan δ at 10^3 as a function of frequency.

Ta) co-doped TiO_2.[37] As shown in the inset of Fig. 5, the tan δ values of the CTTO and ACTTO-1 are huge (>0.1), which is unsuitable for capacitor applications.[2,42] This observation has never been explained in detail. Surprisingly, when increasing the Al^{3+}/Cr^{3+} ratio to 1.0 ($x = 0.025$), the large ε' of $\sim 6 \times 10^4$ with a low tan δ of $\sim$0.07 was obtained. Such a large ε' of ACTTO-2 can be comparable to those observed in several co-doped TiO_2 ceramics.[5,8,9,13,14,21,22,25,27–29,35,38] Furthermore, the rapid decrease in ε' is observed at the frequency range of 10^4 Hz, indicating the additional polarization in the low-frequency range below 10^4 Hz. This result is caused by the replacement of a half Cr^{3+} with Al^{3+} ions. The significantly increased ε' of ACTTO-2 may be correlated to a change in the charge compensation in the rutile-TiO_2 structure, which were triple-doped with Al^{3+}, Cr^{3+}, and Ta^{5+}.

Fig. 6 shows the temperature dependence of dielectric properties for all the samples. The ε' values of CTTO and ACTTO-1 are strongly dependent on the temperature in the range from −60 to 210 °C. Notably, ACTTO-2 shows better temperature stability of ε' than CTTO and ACTTO-1. As depicted in the inset of Fig. 6, two relaxation peaks of tan δ around 0 °C and 150 °C can be observed in the CTTO and ACTTO-1 samples, while only a low-temperature relaxation peak of the ACTTO-2 sample was observed. A low-temperature relaxation is likely

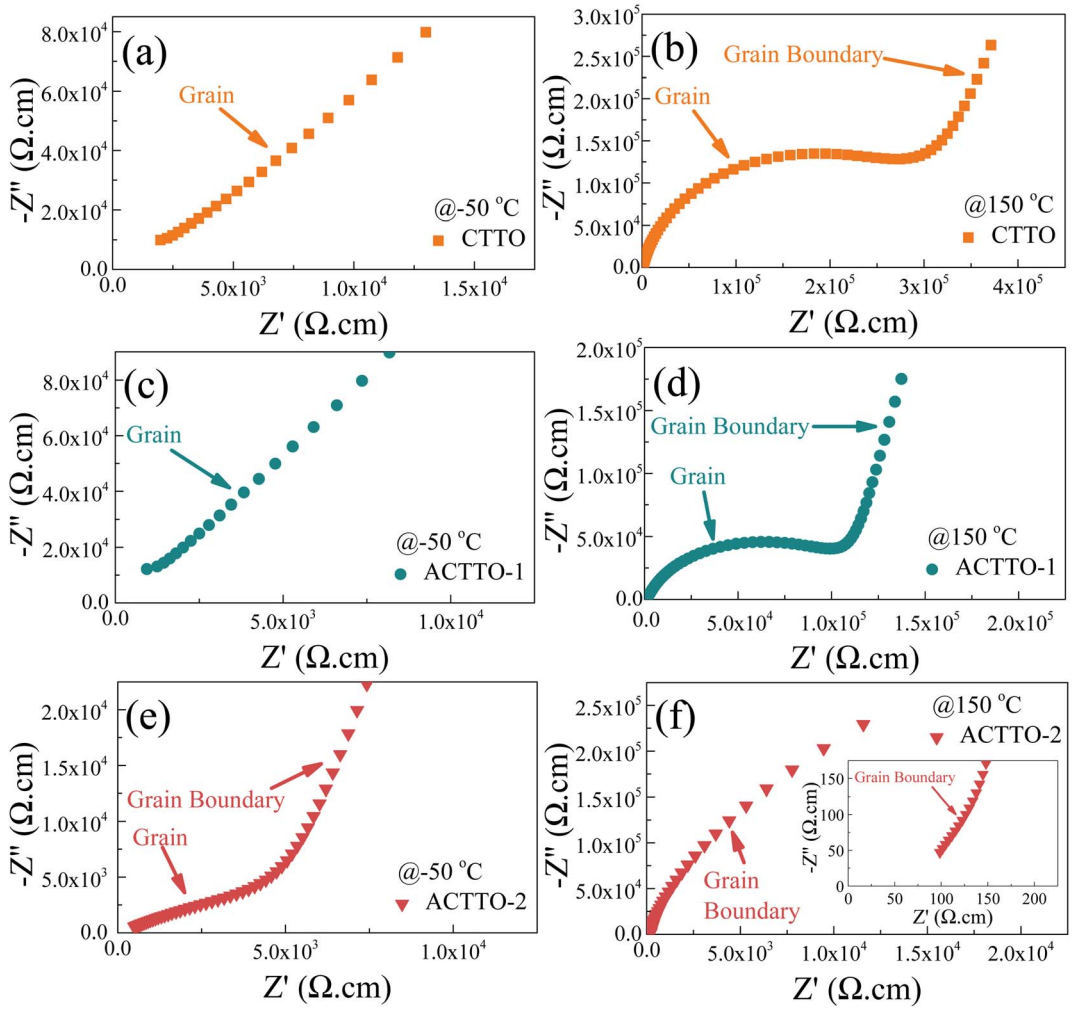

Fig. 7 Impedance complex plane (Z^*) plots at 50 °C and 150 °C of (a and b) CTTO, (c and d) ACTTO-1, and (e and f) ACTTO-2 ceramics; inset of (f) shows Z^* plots at high frequencies.

associated with the dielectric response at the internal interfaces such as GBs and/or surface layer.[2,27]

To clarify the origin of the abnormally enhanced GD properties of ACTTO-2 compared to that of CTTO and ACTTO-1, impedance spectroscopy was used to examine the electrical properties of the grains and GBs.[5,7,32,35] As shown in Fig. 7(a) and (c), at −50 °C, a nonzero intercept on the Z' axis in the complex impedance plane (Z^*) of the CTTO and ACTTO plots disappeared. Only a part of a semicircular arc due to the grain response at high frequencies was found, indicating a large resistivity of the grains.[43] When the measuring temperature was increased to 150 °C, the semicircular arc of the grain response can be observed in the Z^* plots of CTTO and ACTTO-1. Furthermore, a tail of the relatively large semicircular arc of the GBs was observed.[43] At 150 °C, the R_g values for CTTO and ACTTO-1 are about 3.5×10^5 and 1.2×10^5 Ω, respectively, indicating that the grains of these two samples are the insulators. This result indicates that there are no semiconducting grains in CTTO and ACTTO-1.[1,43] For the In^{3+}/Nb^{5+} co-doped TiO_2,[1] although the grains are insulators, the GD response was observed due to the creation of EPDDs. From the first principles calculation and impedance spectroscopy, the EPDDs and strong interfacial polarization cannot be pronounced in CTTO and ACTTO, giving rise to a low ε' value. According to the previous study,[37] we found that the semiconducting grains, which were confirmed by the observed nonzero intercept in Z^* plots, can be created in the 1.0%(Cr + Ta) co-doped TiO_2 sintered at 1400–1500 °C. This result means that there were no free charge carriers in the grains of CTTO and ACTTO-1. It is likely that with the increase in the co-doping concentration of Cr and Ta, self-charge compensation may occur, which can be expressed as follows:[44]

$$Ta_2O_5 + Cr_2O_3 \xrightarrow{4TiO_2} 2Ta_{Ti}^{\bullet} + 2Al_{Ti}^{'} + 8O_O \quad (2)$$

The charge balance equation of the 10%(Cr + Ta) co-doped TiO_2 can be expressed as $[Cr_{0.05}{}^{3+}Ta_{0.05}{}^{5+}]Ti_{0.9}{}^{4+}O_{12}$. As summarized in Table 2, the R_g value of ACTTO-1 was reduced by a factor of ~3 compared to that of CTTO. This result indicates that the replacement of Cr^{3+} with a small amount of Al^{3+} can cause an increase in the free charge carriers inside the grains. Furthermore, the conduction activation energies of the insulating grains (E_i) of CTTO and ACTTO-1 were calculated to be 0.705 and 0.686 eV, respectively. This decreased E_i is consistent with the observed decrease in R_g.

In contrast to those of CTTO and ACTTO-1, as shown in Fig. 7(e), a small arc can be observed in the Z^* plot of the ACTTO-2 at −50 °C with R_g of $\sim 5 \times 10^3$ Ω. At 150 °C, the large arc and nonzero intercept can be observed, as shown in Fig. 7(f) and its inset, respectively. The R_g value of ACTTO-2 was extremely reduced by three orders of magnitude compared to those of CTTO and ACTTO-1. The insulating grins of CTTO can be transformed to semiconducting grains by replacing a half of Cr^{3+} with Al^{3+}.[43] Therefore, the GD properties of ACTTO-2 are attributed to the interfacial polarization at internal interfaces such as insulating GBs and insulative outer surface layer.[31,32,35]

An applied electric field forces a large number of free charges in the semiconducting grains to move and accumulate at the insulating GB layers or surface layers, giving rise to the significantly increased ε'. According to the previous work[6] and the first principles calculation in this study, the Al^{3+} doping ions did not prefer to occupy at the Ti^{4+} sites due to a relatively smaller ionic radius of Al^{3+}. Instead, the Al^{3+} ions behave as interstitial ions. Thus, the charge compensation in the $Al_{0.025}Cr_{0.025}Ta_{0.05}Ti_{0.9}O_2$ composition (ACTTO-2) has been re-balanced due to a relatively high concentration of the donor Ta^{5+} doping ions compared to that of the acceptor Cr^{3+} doping ions since Al^{3+} prefers to act as an interstitial ion rather than the doping ion. Accordingly, the self-charge compensation partially occurred, following the relationship $Al_{0.025}{}^{3+}[Cr_{0.025}{}^{3+}Ta_{0.025}{}^{5+}][Ta_{0.025}{}^{5+}Ti_{0.025}{}^{3+}Ti_{0.925}{}^{4+}]O_{12.0375}$. Free electrons can be produced by the excessive Ta^{5+} doping ions (2.5%), following the equations:[25,26]

$$2TiO_2 + Ta_2O_5 \xrightarrow{4TiO_2} 2Ta_{Ti}^{\bullet} + 2Ti_{Ti}^{'} + 8O_O + 0.5O_2 \quad (3)$$

$$Ti^{4+} + e^- \rightarrow Ti^{3+} \quad (4)$$

It is important to note that the critical role of the Al^{3+} doping ions is to produce the insulating layers on the outer surface[6] and/or at the GBs.[5,7] Song *et al.*[7] have suggested that the Al^{3+} doping ions in $Al_xNb_{0.03}Ti_{0.97-x}O_2$ did not prefer to create a $2Al^{3+} + V_O^{\bullet\bullet} + 2Ti^{3+} + 2Nb^{5+} + Ti^{4+}$ structure. Hence, the role of Al^{3+} was not to form the EPDD in the rutile structure. They suggested that Al^{3+} acted as an acceptor dopant and captured the free electrons, which were produced by Nb^{5+}. It is worth noting that the use of organic solvents such as ethanol in the milling process with precursors can generate surface defects.[45]

Furthermore, the substitution of TiO_2 with Al^{3+} can produce the concentration gradient of Ti^{3+} from the outer surface to the inner core.[6] No Ti^{3+} was detected on the outer surface, while more Ti^{3+} detected in the inner core. Fig. 8(a) and (b) show the XPS spectra of Ti 2p for the CTTO and ACTTO ceramics. As expected, Ti^{3+} cannot be fitted in the XPS spectra. For the CTTO ceramic, the disappearance on Ti^{3+} is due to the self-charge compensation between the Cr^{3+} and Ti^{5+} dopants, confirming the insulating grains in the Z^* plot of the CTTO. On the other hand, for the ACTTO-2 ceramic, Al^{3+} doping into may cause the composition gradient of Ti^{3+} and Ti^{4+}, just as reported in the Al^{3+}/Nb^{5+} co-doped TiO_2.[6] The remarkably enhanced dielectric response in the triple-doped ceramic is therefore attributed to the re-balancing charge compensation. Fig. 8(c) and (d) illustrate the XPS spectra of O 1s of the CTTO and ACTTO-2 ceramics, respectively. For the CTTO and ACTTO-2 samples, the peak that referred to oxygen lattice (Ti–O) appeared at the binding energies of 529.94 and 530.15 eV, respectively.[5,7,10,25] The oxygen vacancy ($V_O^{\bullet\bullet}$) peak of the CTTO and ACTTO-2 samples was found at the binding energies of 531.68 and 531.89 eV,[1,25] respectively. The percentage ratios of the $V_O^{\bullet\bullet}$ and oxygen lattice for the CTTO and ACTTO-2 ceramics were about 8.90% and 13.03%, respectively. It is likely that the detected $V_O^{\bullet\bullet}$ in the CTTO and ACTTO-2 ceramics may be caused by oxygen loss during the sintering at a high temperature.[4,33] According to the impedance spectroscopy, the semiconducting grains of the

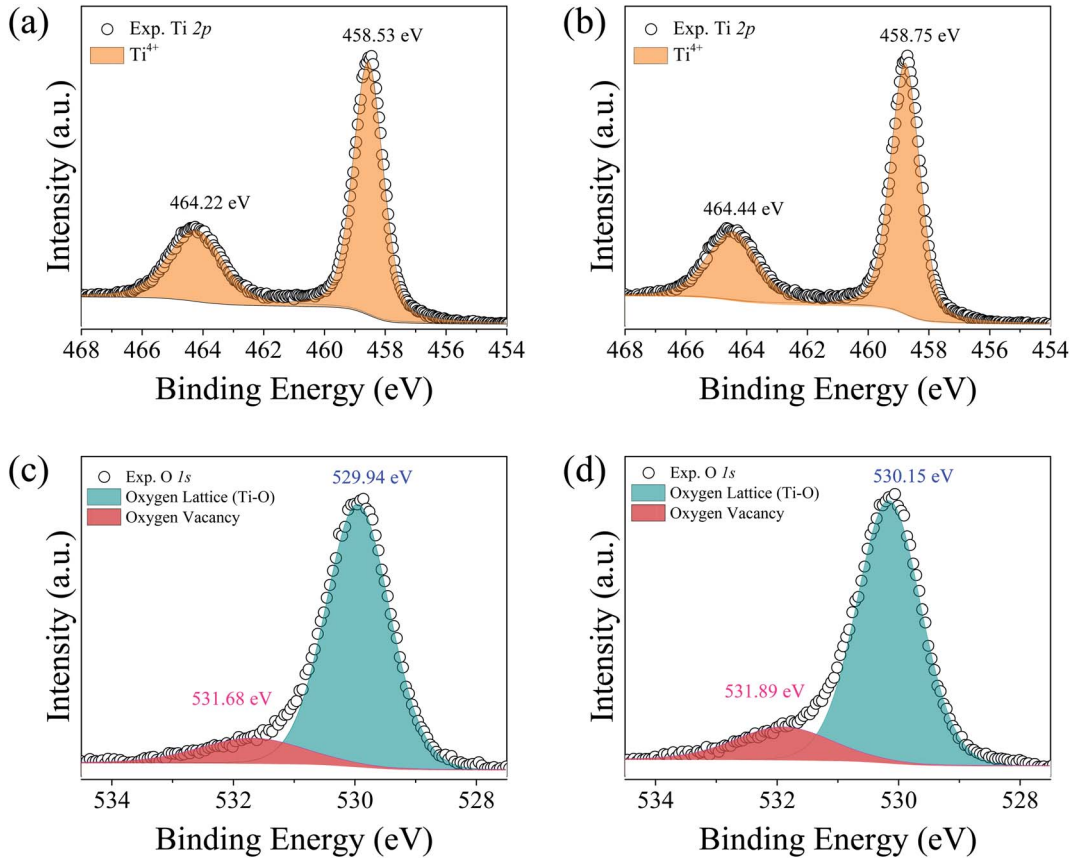

Fig. 8 XPD spectra of Ti 2p for (a) CTTO and (b) ACTTO-2 ceramics and O 1s for (c) CTTO and (d) ACTTO-2 ceramics.

CTTO ceramic was not formed due to the self-charge compensation between the dopants. Therefore, the disappearance of Ti^{3+} was likely caused by the charge compensation between Ti vacancy (V''_{Ti}) and $V^{\cdot\cdot}_{O}$. According to the XPS results, the relative atomic percentage (%) ratio of Cr/Ta/Ti in the CTTO ceramic is 0.092/0.089/1.00, while that of the ACTTO-2 ceramic is 0.112/0.108/0.122/1.00. The Cr/Ti and Ta/Ti ratios of the CTTO ceramic are slightly higher than those of the theoretical ratio. It was found that the Al/Ti and Cr/Ti ratios of the ACTTO-2 ceramic are much higher than that of the theoretical ratio. Thus, this result may confirm the hypothesis that Al preferred to segregate near the surface on the ACTTO ceramics.

4. Conclusions

The charge compensation of the $(Al_xCr_{0.05-x})Ta_{0.05}Ti_{0.9}O_2$ ceramics was re-balanced by increasing the Al^{3+}/Cr^{3+} ratio to increase ε'. The increased Al^{3+}/Cr^{3+} ratio caused a slight change in the mean grain size but had a pronounced effect on the densification process. The self-charge compensation between Cr^{3+}–Ta^{5+} in $(Cr_{0.05})Ta_{0.05}Ti_{0.9}O_2$ did not cause significant increase in the GD response due to the absence of Ti^{3+} (or very small amount) because it has a ε' value of $\sim 10^3$. The low ε' value was due to a large R_g and very high conduction activation of the grains, which can create the interfacial polarization. Nevertheless, the ultra-high $\varepsilon' \sim 6.68 \times 10^4$ can be achieved by re-balancing the charge compensation *via* the partial replacement of Cr^{3+} with Al^{3+} with the Al^{3+}/Cr^{3+} ratio of 1.0. The semiconducting grains can be produced due to the interstitial Al^{3+} ions. Hence, the self-charge compensation (Cr^{3+}–Ta^{5+}) has partially existed, and the Ta^{5+} left can produce the semiconducting grains. The GD properties were therefore attributed to the interfacial polarization at the interface between the semiconducting and insulating parts, as supported by impedance spectroscopy.

Conflicts of interest

The authors declare no competing financial interests.

Acknowledgements

This project is funded by the National Research Council of Thailand (NRCT): (N41A640084). This work has also received funding support from the Fundamental Fund of Khon Kaen University and the National Science, Research and Innovation Fund (NSRF). P. Siriya expresses her gratitude to the Science Achievement Scholarship of Thailand (SAST) for a PhD scholarship in Physics.

References

1 W. Hu, Y. Liu, R. L. Withers, T. J. Frankcombe, L. Norén, A. Snashall, M. Kitchin, P. Smith, B. Gong, H. Chen,

J. Schiemer, F. Brink and J. Wong-Leung, *Nat. Mater.*, 2013, **12**, 821–826.
2 W. Tuichai, S. Danwittayakul, N. Chanlek, P. Srepusharawoot, P. Thongbai and S. Maensiri, *RSC Adv.*, 2017, **7**, 95–105.
3 J. Li, Z. Xu, F. Li, X. Zhu and S. Zhang, *RSC Adv.*, 2016, **6**, 20074–20080.
4 W. Tuichai, S. Danwittayakul, S. Maensiri and P. Thongbai, *RSC Adv.*, 2016, **6**, 5582–5589.
5 G. Liu, H. Fan, J. Xu, Z. Liu and Y. Zhao, *RSC Adv.*, 2016, **6**, 48708–48714.
6 W. Hu, K. Lau, Y. Liu, R. L. Withers, H. Chen, L. Fu, B. Gong and W. Hutchison, *Chem. Mater.*, 2015, **27**, 4934–4942.
7 Y. Song, X. Wang, X. Zhang, Y. Sui, Y. Zhang, Z. Liu, Z. Lv, Y. Wang, P. Xu and B. Song, *J. Mater. Chem. C*, 2016, **4**, 6798–6805.
8 W. Dong, W. Hu, A. Berlie, K. Lau, H. Chen, R. L. Withers and Y. Liu, *ACS Appl. Mater. Interfaces*, 2015, **7**, 25321–25325.
9 W. Tuichai, S. Danwittayakul, J. Manyam, N. Chanlek, M. Takesada and P. Thongbai, *Materialia*, 2021, **18**, 101175.
10 W. Tuichai, S. Danwittayakul, N. Chanlek, P. Thongbai and S. Maensiri, *J. Alloys Compd.*, 2017, **703**, 139–147.
11 T. Nachaithong, W. Tuichai, P. Moontragoon, N. Chanlek and P. Thongbai, *Ceram. Int.*, 2018, **44**, S186–S188.
12 T. Nachaithong, P. Moontragoon, N. Chanlek and P. Thongbai, *RSC Adv.*, 2020, **10**, 24784–24794.
13 M.-Y. Tse, X. Wei and J. Hao, *Phys. Chem. Chem. Phys.*, 2016, **18**, 24270–24277.
14 M.-Y. Tse, M.-K. Tsang, Y.-T. Wong, Y.-L. Chan and J. Hao, *Appl. Phys. Lett.*, 2016, **109**, 042903.
15 N. Thongyong, W. Tuichai, N. Chanlek and P. Thongbai, *Ceram. Int.*, 2017, **43**, 15466–15471.
16 X. Wei, W. Jie, Z. Yang, F. Zheng, H. Zeng, Y. Liu and J. Hao, *J. Mater. Chem. C*, 2015, **3**, 11005–11010.
17 C. Zhao and J. Wu, *ACS Appl. Mater. Interfaces*, 2018, **10**, 3680–3688.
18 Z. Cao, J. Zhao, J. Fan, G. Li and H. Zhang, *Ceram. Int.*, 2021, **47**, 6711–6719.
19 C. Yang, M.-Y. Tse, X. Wei and J. Hao, *J. Mater. Chem. C*, 2017, **5**, 5170–5175.
20 N. Thongyong, P. Srepusharawoot, W. Tuichai, N. Chanlek, V. Amornkitbamrung and P. Thongbai, *Ceram. Int.*, 2018, **44**, S145–S147.
21 P. Liang, J. Zhu, D. Wu, H. Peng, X. Chao and Z. Yang, *J. Am. Ceram. Soc.*, 2021, **104**, 2702–2710.
22 X. Zhou, P. Liang, J. Zhu, Z. Peng, X. Chao and Z. Yang, *Ceram. Int.*, 2020, **46**, 11921–11925.
23 W. Li, Z. Liu, F. Zhang, Q. Sun, Y. Liu and Y. Li, *Ceram. Int.*, 2019, **45**, 11920–11926.
24 Z. Liu, C. Zhao, B. Wu and J. Wu, *Phys. Chem. Chem. Phys.*, 2018, **20**, 21814–21821.
25 W. Tuichai, N. Thongyong, S. Danwittayakul, N. Chanlek, P. Srepusharawoot, P. Thongbai and S. Maensiri, *Mater. Des.*, 2017, **123**, 15–23.
26 W. Tuichai, S. Danwittayakul, N. Chanlek and P. Thongbai, *Mater. Res. Bull.*, 2019, **116**, 137–142.
27 N. Thongyong, N. Chanlek, P. Srepusharawoot and P. Thongbai, *Molecules*, 2021, **26**, 6952.
28 W. Dong, D. Chen, W. Hu, T. J. Frankcombe, H. Chen, C. Zhou, Z. Fu, X. Wei, Z. Xu, Z. Liu, Y. Li and Y. Liu, *Sci. Rep.*, 2017, **7**, 9950.
29 T. Nachaithong, N. Chanlek, P. Moontragoon and P. Thongbai, *Molecules*, 2021, **26**, 3230.
30 Z. Li and J. Wu, *J. Materiomics*, 2017, **3**, 112–120.
31 T. Nachaithong, P. Kidkhunthod, P. Thongbai and S. Maensiri, *J. Am. Ceram. Soc.*, 2017, **100**, 1452–1459.
32 T. Nachaithong, P. Thongbai and S. Maensiri, *J. Eur. Ceram. Soc.*, 2017, **37**, 655–660.
33 Y. Q. Wu, X. Zhao, J. L. Zhang, W. B. Su and J. Liu, *Appl. Phys. Lett.*, 2015, **107**, 242904.
34 J. Li, F. Li, C. Li, G. Yang, Z. Xu and S. Zhang, *Sci. Rep.*, 2015, **5**, 8295.
35 W. Tuichai, S. Danwittayakul, N. Chanlek and P. Thongbai, *J. Alloys Compd.*, 2017, **725**, 310–317.
36 V. Bovtun, J. Petzelt, M. Kempa, D. Nuzhnyy, M. Savinov, S. Kamba, S. M. M. Yee and D. A. Crandles, *Phys. Rev. Mater.*, 2018, **2**, 075002.
37 W. Tuichai, S. Danwittayakul, N. Chanlek, M. Takesada, A. Pengpad, P. Srepusharawoot and P. Thongbai, *ACS Omega*, 2021, **6**, 1901–1910.
38 W. Tuichai, S. Danwittayakul, P. Srepusharawoot, P. Thongbai and S. Maensiri, *Ceram. Int.*, 2017, **43**, S265–S269.
39 R. D. Shannon, *Acta Crystallogr., Sect. A*, 1976, **32**, 751–767.
40 C. C. Homes and T. Vogt, *Nat. Mater.*, 2013, **12**, 782–783.
41 M. N. Rahaman, *Ceramic processing and sintering*, M. Dekker, New York, 2nd edn, 2003.
42 Y. Wang, W. Jie, C. Yang, X. Wei and J. Hao, *Adv. Funct. Mater.*, 2019, **29**, 1808118.
43 M. Li and D. C. Sinclair, *J. Appl. Phys.*, 2013, **114**, 034106.
44 J. Boonlakhorn, N. Chanlek, J. Manyam, P. Srepusharawoot, S. Krongsuk and P. Thongbai, *J. Adv. Ceram.*, 2021, **10**, 1243–1255.
45 J. L. Clabel H, I. T. Awan, A. H. Pinto, I. C. Nogueira, V. D. N. Bezzon, E. R. Leite, D. T. Balogh, V. R. Mastelaro, S. O. Ferreira and E. Marega, *Ceram. Int.*, 2020, **46**, 2987–3001.